Catalysis Communications 171 (2022) 106518

Contents lists available at ScienceDirect

Catalysis Communications

journal homepage: www.elsevier.com/locate/catcom

Photocatalytic degradation of methylene blue using monometallic and bimetallic Bi-Fe doped TiO_2

Saurav Mishra [a], Nandana Chakinala [b], Anand G. Chakinala [b,*], Praveen K. Surolia [a,*]

[a] Solar Energy Conversion and Nanomaterials Laboratory, Department of Chemistry, Manipal University Jaipur, Jaipur 303007, Rajasthan, India
[b] Chemical Reaction Engineering Laboratory, Department of Chemical Engineering, Manipal University Jaipur, Jaipur 303007, Rajasthan, India

ARTICLE INFO

Keywords:
Photocatalytic degradation
M-doped TiO_2 (M-Bi-Fe)
Methylene blue
Wet impregnation

ABSTRACT

This work reports synthesis and characterization of mono and bimetal doped TiO_2-based photocatalyts using Bi and Fe metals prepared via wet impregnation method. Photocatalytic performances of the synthesized catalysts were tested for the degradation of methylene blue. Results revealed that 1%Bi/TiO_2 (*w*/w) exhibited best photocatalytic performance and achieved 80% degradation of 50 ppm MB solution within two hours. The monometallic doping showed better performance than the bimetallic doping of Bi and Fe. This diminished performance with co-doping was due to the agglomeration effect which accelerates recombination of electrons and holes. First order-kinetic model was used for the study of degradation.

1. Introduction

The rapid and extensive rise in industrial activities has led to a greater environmental concern, due to the impact on surface water as well as human health. Industrial effluents have been noticed to their long-term adverse effects on human life and aquatic organisms [1,2]. The photocatalytic degradation technique has gained interest due to its effectiveness for removal of industrial effluents [3–5]. Further, semiconductors heterogeneous photocatalysts such as TiO_2, ZnO, Fe_2O_3, and CdS etc., are used for the purpose, without or with modifications like, through the combination of semiconductors or doping of metals or non-metals to improve their photocatalytic performance. These modifying processes are emphasized as vital tools to enhance the photocatalytic performance to degrade organic pollutants effectively with the model of the zero-waste scheme [6–8]. TiO_2 catalyst is considered as one of the best semiconductor and frequently used to degrade the organic matter owing to impressive photocatalytic processibility and remarkable stability [9,10]. Nevertheless, its wide bandgap (E_g = 3.2 eV) is not approachable in the solar spectrum hence, it has been imperative to prepare novel photocatalysts for the proper working in visible light conditions achieving lower bandgap [11]. Along with that, minimising the recombination of generated charge carriers, electrons and holes is a huge challenge. Thus, several mono and bimetal doped TiO_2 catalysts has been widely studied to improve its photocatalytic activity [12–14]. Bismuth-based photocatalytic has achieved considerable attention owing to its low toxicity, higher stability, low cost, and expressed exclusive photocatalytic activity with reducing gap amid valence and conductive band, as well as minimise the recombination of charge carriers [15]. Nadia Riaz et.al, have fabricated bimetallic materials Cu, Ni/TiO_2 photocatalyst through wet impregnation for degrading methyl orange varying operational parameters such as photocatalyst loading, pollutant concentration, and irradiation time [16]. Praveen K. Surolia et al. has prepared β-cyclodextrin CuO/ZnO Nanocomposite and studied photocatalytic performance for model textile dyes pollutants degradation, malachite green (MG), and methylene blue (MB). In addition, the prepared catalyst encompasses exterior and interior cavity which can encapsulate pollutant molecules [13]. PAK Reddy et al. fabricated bismuth doped TiO_2 based materials for the degradation of isoproturon herbicide under solar light irradiation [17]. Bismuth doped TiO_2 species could be playing key role in reducing recombination of electron-hole, thus doped TiO_2 catalyst expressed appreciable photocatalyst performance rather pure TiO_2. Rajesh J. Tayade et al. synthesized bismuth doped TiO_2 nanotube using sol-gel and hydrothermal methods and employed for the degradation of rhodamine-B dyes under sunlight irradiation [18].

Doping of Fe was also observed to enhance the photocatalytic activity of TiO_2. Jyun-Hong Shen et al. prepared Fe-doped TiO_2 based materials and employed for the degradation azo dyes [19]. The dopant iron expressed the synergetic effect with producing extra hydroxyl group radical for leading dyes degradation under visible light. Praveen K

* Corresponding authors.
E-mail addresses: anandgupta.chakinala@jaipur.manipal.edu (A.G. Chakinala), praveenkumar.surolia@jaipur.manipal.edu (P.K. Surolia).

https://doi.org/10.1016/j.catcom.2022.106518
Received 10 August 2022; Received in revised form 14 September 2022; Accepted 22 September 2022
Available online 23 September 2022

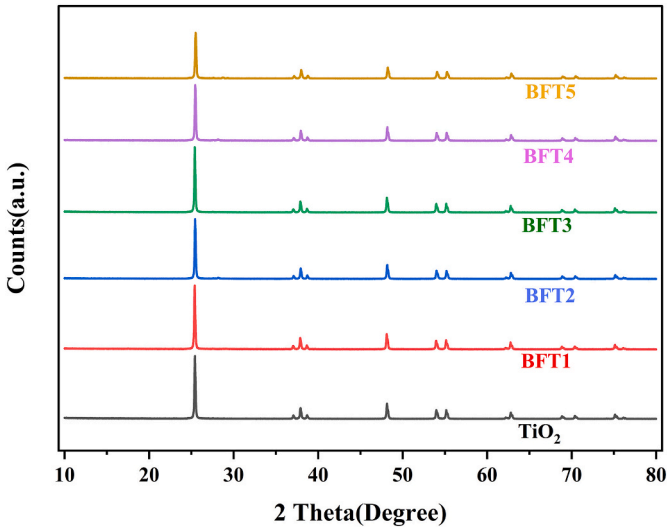

Fig. 1. XRD pattern for commercial and modified TiO_2 catalysts.

Surolia et al. reported enhanced activity for the photocatalytic degradation of acetophenone when TiO_2 was doped with Fe using wet impregnation method [20].

In this work, we have synthesized mono, and bimetal (Bi, Fe) doped TiO_2 materials through the wet impregnation method for the degradation of methylene blue (MB) under UV light [21,22]. The prepared catalytic materials were characterized using XRD, FT-IR, SEM, DRS, PL and TGA. These materials were applied to degrade model dye pollutant MB in aqueous media. As per our best knowledge, the bimetallic doping of Bi and Fe in combination has not been reported so far for the purpose of photocatalytic degradation of organic pollutants in water.

2. Experimental section

2.1. Synthesis of catalysts

The catalytic preparation process is provided in supporting information and schematically illustrated in Fig. S1. Catalysts were synthesized via wet impregnation technique. The catalysts synthesized with % loading of Bi:Fe (*w*/w) on TiO_2 were (1.0:0.0); (0.75:0.25); (0.50:0.50); (0.25:0.75); (0.0:1.0) and named as BFT1, BFT2, BFT3, BFT4, and BFT5 respectively.

2.2. Catalyst characterization

The prepared catalysts were characterized using different analysis techniques such as XRD, DRS, FT-IR, TGA, SEM, PL and details are provided in supporting information.

2.3. Experimental setup and photocatalytic degradation experiment

The photocatalytic reaction was carried out using a 500 mL reactor set-up consisting of 250 W mercury vapor lamp (fig. S2). Photocatalytic performance of the prepared catalysts was evaluated by measuring the concentration decrease of MB in the reaction solution. Details of the experimental setup and reaction conditions are provided in supporting information.

3. Result and discussion

3.1. X-ray diffraction analysis (XRD)

The XRD patterns of commercial and modified TiO_2 catalysts are shown in Fig. 1. The maximum intense peak was observed at $2\theta = 25.3$

Table 1
Textural and electronic properties of bare and bi-metallic doped TiO_2 catalysts and their performance analysis.

Catalyst	Average crystallite size (nm)	Band gap, E_g (eV)	% Degradation (After 120 min)	Initial rate[a] × 10^{-5} [mol L^{-1} min^{-1}]	Rate constant[a] (K_{app}) × 10^{-2} [min^{-1}]	R^2
Blank	–	–	43	0.8	0.52	0.99
TiO_2	28.74	3.23	66	2.4	1.3	0.96
BFT1	29.05	3.20	80	1.9	1.2	0.99
BFT2	28.64	3.19	45	0.9	0.64	0.99
BFT3	29.03	3.24	48	1.0	0.66	0.99
BFT4	28.84	3.25	55	1.1	0.67	0.99
BFT5	27.36	3.26	59	1.4	0.82	0.99

[a] Calculated using UV–Vis absorbance data.

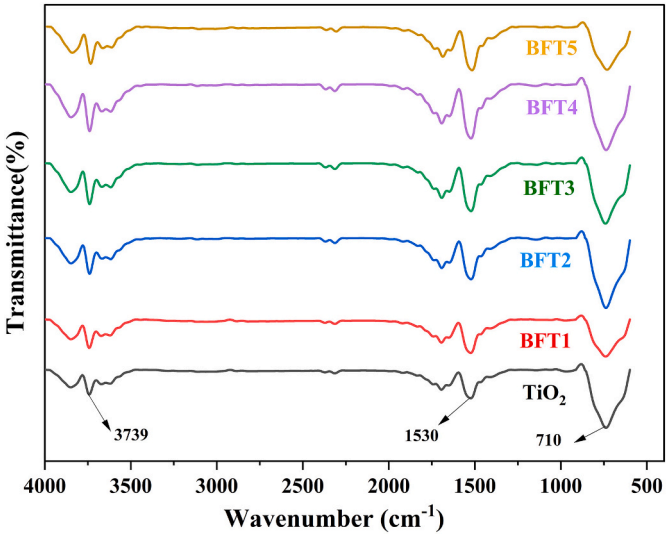

Fig. 2. FT-IR spectra of commercial and modified TiO_2 catalysts.

in all the XRD patterns which confirmed the existence of primarily anatase phase [23]. Major diffraction peaks in XRD pattern of all the catalyst were observed at $2\theta = 25.3^0$, 36.9^0, 37.7^0, 38.7^0, 48.1^0, 54.08^0, 55.1^0, 70.5^0, 75.1^0, which are corresponding to (101), (103), (004), (112), (200), (105), (211), (213), and (116). Bi and Fe metal impregnation on TiO_2 surfaces did not create any extra peak. That could be due to the smaller loading values of Bi and Fe metals (less than 1% *w*/w). Higher peak intensities indicate that all the catalysts are having crystalline nature. The crystallite sizes were calculated for BFT1, BFT2, BFT3, BFT4, BFT5, and TiO_2 as 29.05, 28.64, 29.03, 28.85, 27.37, and 28.75, respectively (Table 1). These crystallite sizes were determined from the characteristic peak of $2\theta = 25.3$ (101) for the anatase phase using the Scherrer formula, with a shape factor (K) of 0.9: (Eq. (1)) [7]. All these crystallite sizes are in similar range which confirms no considerable change due to doping of metals in TiO_2.

$$Crystallite\ size = K\lambda/(W cos\theta) \quad (1)$$

where $W = W_b - W_s$. W_b is the broadened profile width of experimental sample. W_s is the standard profile width of reference silicon sample, and λ is the wavelength of X-ray radiation.

3.2. Infrared spectroscopy analysis (FTIR)

FTIR analysis of all the catalysts was performed and the obtained spectra are shown in Fig. 2. It was observed that all the catalysts have shown broad peak between 550 and 800 cm^{-1}. This includes stretching

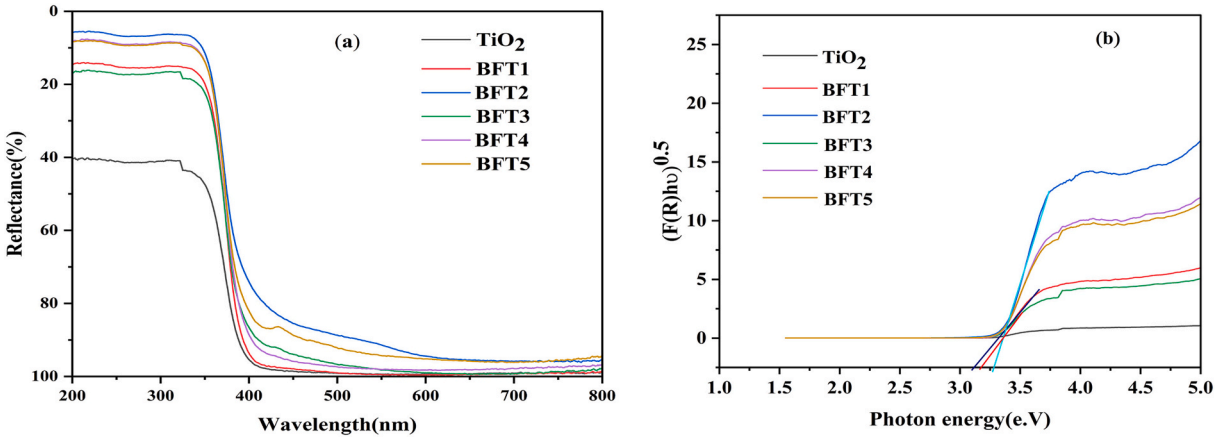

Fig. 3. (a) DRS spectra of commercial TiO_2 and their modified moieties and (b) band-gap energy from $\{(R)^* h\upsilon\}^{1/2}$ with photon energy ($h\upsilon$).

vibrations of Ti-O bond and Ti–O–Ti bond [24]. The peaks at 3600–3800 cm^{-1} range is due to stretching of –OH groups. All the catalyst showed two medium bands in 1500–1700 cm^{-1} due to the deformation vibration of adsorbed water molecules [25,26]. The absence of any peak around 1200 cm^{-1} is attributed to the doping done on the TiO_2 lattice [22].

3.3. Diffuse reflectance spectra analysis (DRS)

The optical absorption properties of pure and impregnated TiO_2 photocatalysts were studied with diffuse reflectance UV–Visible spectroscopy (Fig. 3). The study clearly shows that after doping with bismuth and iron there was no considerable change observed in the bandgap (Table 1). The bandgap was calculated with the help of Kubelka-Munk equation using DRS data analysis (Eq. (2)) [27].

$$\left[F(R) = \left[\frac{(1-R^2)}{2R}\right]\right] \tag{2}$$

where R is the measured absolute reflectance of the photocatalyst. Fig. 3 (b) presents the Kubelka-munk plots for pure and doped photocatalyst.

3.4. Scanning electron microscopy analysis (SEM)

SEM analysis was used to study the texture and morphology of synthesized photocatalysts (Fig. S3). All the catalyst were observed in spherical shape with typical size in the range of less than 100 nm and facilitating a better uniform distribution. No change in morphology was observed after metal loading. The existence of metals after loading was confirmed using EDX analysis (Fig. S4). However, EDX analysis could provide the results for the metal particles which were existing only on the TiO_2 surface.

3.5. Photoluminescence spectral analysis (PL)

PL spectra showcase efficiency of transferring charge carrier in semiconductor materials which help to get the information about separation and recombination of photo generated electron pair. Photocatalytic activities of various catalysts are distinct in term of charge carriers (e^-/h^+ pair) recombination rate. In this context, the higher PL intensity render the higher recombination rate of electron-hole (e^-/h^+) which is attributed to reduce the photocatalytic activities of catalysts [28–30]. The photoluminescence intensity of commercially TiO_2 was observed higher, so recombination rate of charge carriers was to be high compared to other synthesized catalysts. The PL spectrum of all the synthesized catalysts is shown in Fig. S5.

3.6. Thermogravimetric analysis (TGA)

The thermal behaviour of synthesized catalysts was demonstrated by the TGA spectrum that confirms the commendable thermal stability of all the catalysts (Fig. S6). There was a smaller weight loss observed starting around, that discloses the mainly moisture removal and some of the impurity which might have left in the sample during the doping of

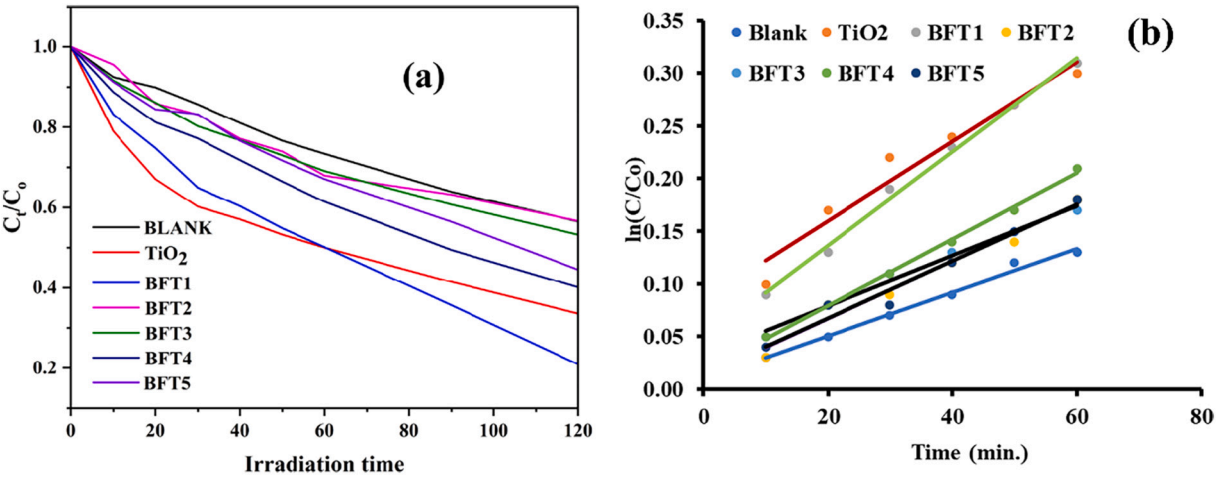

Fig. 4. (a) Decrease in concentration of MB as a function of irradiation time, (b) kinetics of MB degradation.

the metals [31,32]. However, in all the cases, weight loss was less than 5%.

4. Photocatalytic activity and kinetics of methylene blue degradation

The photocatalytic degradation study of the synthesized catalysts was conducted for the degradation of MB solution and the results are provided in Table 1. A 500 mL 50 ppm solution of MB was taken in the photochemical reactor and a catalyst dose of 0.2 g/L was used in all the performed experiments. The removal of MB due to adsorption was observed as in the range of 8 to 15% only with all the catalysts. The initial rate of reaction was observed highest for the commercial TiO_2 followed by BFT1 that contains 1%Bi in TiO_2 (*w*/w) (Table 1). This initial rate of degradation was calculated at time 10 min of the reaction. However, final percentage of degradation was observed 80% with BFT1 and 66% with commercial TiO_2 which were highest among other catalysts applied after 2 h (Table 1 and Fig. S7). The final percentage degradation was observed in the range of 43 to 80% for all the reactions performed. For comparison with BFT1, the performance of some selected previously reported TiO_2 based photocatalysts for MB degradation is mentioned in table S1.

Comparison of photocatalytic performance of TiO_2, BFT1, BFT2, BFT3, BFT4, and BFT5 validates that the BFT1 express the higher extent of photocatalytic performance rather than other photocatalysts. In other metal doped TiO_2 catalysts, the addition of Fe content decrease the performance as the Fe dopant possesses the multivalency and lesser number of redox potential (−0.44) which leads to the agglomeration and recombination of electrons and holes [33]. Thus, the Fe ions turn into the recombination centres for the electrons and holes pairs under UV light irradiation [34]. The redox potential of Bi^{3+}/Bi^{+} and Fe^{2+}/Fe are 0.20 and − 0.44 respectively, which leads to electrons transferring from Fe to Bi, that could result of agglomeration action. Thus, we may conclude that the Fe doping in Bi/TiO_2 catalyst leads to antagonist performance. However, agglomeration possibilities in the catalysts modified only with doping of either Fe or Bi metal substantially prevented and lead to better degradation of MB (Table 1). Fig. S8 shows the degradation pattern of MB using BFT1 catalyst under the UV irradiation of 2 h.

The kinetic study of MB degradation is shown in Fig. 4 (a) and 4 (b). For studying degradation rate of dye, we had kept the solution for 30 min. in dark, which is called adsorption time. As per Langmuir-Hinshelwood mechanism, the kinetics follows pseudo-first order kinetics, where the rate of degradation reaction 'r' is proportional to the concentration C_t at time 't' (Eq. (3)) [35].

$$r = \frac{kKC_t}{1 + KC_t} \approx kKC_t = k_{app}C_t \tag{3}$$

where k is the reaction rate constant and K is the reactant adsorption constant. The apparent first order linear transforms are expressed in Fig. 4 (b). The calculated apparent rate constants from slopes and R^2 values of linearity are specified in Table 1. As in Fig. 4 (a), a clear sharp decrease in concentration was observed in initial reaction time in all the reaction performed. The apparent rate constant for degradation of organic compound in various intermediate assigns the faster degradation rate, but not necessarily to the generation of CO_2 ultimately. From Table 1, it can be clearly seen that degradation rate of MB dye is faster for commercial TiO_2 and BFT1 catalysts. The degradation rate constant of the reactions using TiO_2 and BFT1 catalysts are best among all as 1.3×10^{-2} min^{-1} and 1.2×10^{-2} min^{-1} respectively.

5. Mechanistic approaches of photocatalysts in degradation of dye

Aqueous photocatalytic degradation of organic materials can be explained by band- gap model of semiconductors. Semiconductor is composed by band frameworks, valance band (VB) conductance band (CB) separated with an energy gap (E_g) [33]. On the basis of experimental data received, the photocatalysis and mechanistic approaches is proposed. The proposed mechanism of dye degradation using metal doped TiO_2 is given from Eqs. (4)–(10).

$$TiO_2 + hv \rightarrow TiO_2\left(e^{-}_{cb} + h^{+}_{vb}\right) \tag{4}$$

$$TiO_2\left(e^{-}\right) + TM\left(Bi, Fe\right) \rightarrow TiO_2 - M(e^{-}) \tag{5}$$

$$TiO_2 - M(e^{-}) + O_2 \rightarrow TiO_2 - M + O_2^{-\bullet} \tag{6}$$

$$O_2^{-\bullet} + H^{+} \rightarrow HO_2^{\bullet} \tag{7}$$

$$2HO_2^{\bullet} \rightarrow H_2O_2 + O_2 \tag{8}$$

$$H_2O_2 + e^{-}_{cb} \rightarrow OH^{\bullet} + OH^{-} \tag{9}$$

$$OH^{\bullet}/h^{-}_{cb} + Dye \rightarrow Mineralized\ Products \tag{10}$$

Firstly, commercial, and modified TiO_2 photocatalysts takes a photon with energy higher or equal to its band- gap and generate e^{-}/h^{+} charge carriers in CB and VB respectively as in Eqs. (4)–(5). Further, these e^{-} and h^{+} react with the reactive oxygen species O_2 and H_2O, to generate superoxide anion ($^{\bullet}O_2^{-}$), hydroxyl radical ($^{\bullet}OH^{-}$) and H_2O_2 (Eqs. (6)–(9)). These strong oxidative materials that is reactive oxygen species (ROS) further oxidize dye and other organic fragments adsorbed on the photocatalyst, finally to the mineralized products CO_2, H_2O and NH_4^{+} (Eq. (10)). The involvement of these major reactive species can be confirmed by application of suitable scavengers during the process [13].

6. Conclusion

In this work, mono and bimetal doped TiO_2-based photocatalytic materials were synthesized using Bi and Fe metals by wet impregnation method. The degradation of model pollutant MB dye confirmed that 1% Bi/TiO_2 (*w*/w) exhibited best photocatalytic performance compared to other doped TiO_2 photocatalysts and achieved 80% of degradation of 50 ppm MB solution within two hours. The monometallic doping showed better performance than the bimetallic doping of Bi and Fe. This decreased performance with co-doping was due to the agglomeration effect which accelerates the recombination of electrons and holes. Fe dopant holds the multivalency and lesser number of redox potential (−0.44) which leads to the agglomeration and recombination of electrons and holes. Furthermore, this work also fascinated the pseudo-first order kinetic model for assigning degradation rate and mechanistic approach of semiconductors with organic fragments.

Author contribution

Saurav Mishra: Investigation, Data curation, Formal analysis, Write first draft; Nandana Chakinala: Investigation, Editing; Anand G. Chakinala: Conceptualization, Revision, Verification; Praveen K. Surolia: Supervision, Revision. Editing.

Declaration of Competing Interest

The author declare that they have no known competing financial interests or personal relationships that could have appeared to influence the work reported in this paper.

Data availability

Data will be made available on request.

Acknowledgment

Authors thank Manipal University Jaipur for providing the facility for materials characterization. PKS acknowledge the funding support from Science and Engineering Research Board (SERB), India, under Grant No. [EMR/2016/006259].

Appendix A. Supplementary data

Supplementary data to this article can be found online at https://doi.org/10.1016/j.catcom.2022.106518.

References

[1] M.G. Kim, J.M. Kang, J.E. Lee, K.S. Kim, K.H. Kim, M. Cho, S.G. Lee, Effects of calcination temperature on the phase composition, photocatalytic degradation, and Virucidal activities of TiO2 nanoparticles, ACS Omega. 6 (2021) 10668–10678, https://doi.org/10.1021/acsomega.1c00043.

[2] K. Sharma, D. Vaya, G. Prasad, P.K. Surolia, Photocatalytic process for oily wastewater treatment: a review, Int. J. Environ. Sci. Technol. (2022), https://doi.org/10.1007/s13762-021-03874-2.

[3] V.N. Sonkusare, G.R. Chaudhary, G.S. Bhusari, A. Mondal, A.K. Potbhare, Raghvendra K. Mishra, H.D. Juneja, A.A. Abdala, Mesoporous octahedron-shaped Tricobalt tetroxide nanoparticles for photocatalytic degradation of toxic dyes, ACS Omega. 5 (2020) 7823–7835, https://doi.org/10.1021/acsomega.9b03998.

[4] D. Chen, Y. Cheng, N. Zhou, P. Chen, Y. Wang, K. Li, S. Huo, P. Cheng, P. Peng, R. Zhang, L. Wang, H. Liu, Y. Liu, R. Ruan, Photocatalytic degradation of organic pollutants using TiO2-based photocatalysts: a review 268 (2020) 121725, https://doi.org/10.1016/j.jclepro.2020.121725.

[5] D. Gogoi, P. Makkar, N.N. Ghosh, Solar light-irradiated photocatalytic degradation of model dyes and industrial dyes by a magnetic CoFe2O4−gC3N4 S-scheme heterojunction Photocatalyst, ACS Omega. 6 (2021) 4831–4841, https://doi.org/10.1021/acsomega.0c05809.

[6] D. Vaya, P.K. Surolia, Semiconductor based photocatalytic degradation of pesticides: an overview, Environ. Technol. Innov. 20 (2020), 101128, https://doi.org/10.1016/j.eti.2020.101128.

[7] P.K. Surolia, M.A. Lazar, R.J. Tayade, R.V. Jasra, Photocatalytic degradation of 3,3′-Dimethylbiphenyl-4,4′-diamine (o-Tolidine) over Nanocrystalline TiO2 synthesized by sol-gel, solution combustion, and hydrothermal methods, Ind. Eng. Chem. Res. 47 (2008) 5847–5855, https://doi.org/10.1021/ie800073j.

[8] S. Chen, D. Huang, G. Zeng, W. Xue, L. Lei, P. Xu, R. Deng, J. Li, M. Cheng, In-situ synthesis of facet-dependent BiVO4/Ag3PO4/PANI photocatalyst with enhanced visible-light-induced photocatalytic degradation performance: synergism of interfacial coupling and hole-transfer, Chem. Eng. J. 382 (2020), 122840, https://doi.org/10.1016/j.cej.2019.122840.

[9] V. Etacheri, C. Di Valentin, J. Schneider, D. Bahnemann, S.C. Pillai, Visible-light activation of TiO2 photocatalysts: advances in theory and experiments, J Photochem Photobiol C: Photochem Rev 25 (2015) 1–29, https://doi.org/10.1016/j.jphotochemrev.2015.08.003.

[10] P.K. Surolia, R.V. Jasra, Degradation and mineralization of aqueous nitrobenzene using ETS-4 photocatalysis, Desalin. Water Treat. 57 (2016) 15989–15998, https://doi.org/10.1080/19443994.2015.1079801.

[11] O. Fawzi Suleiman Khasawneh, P. Palaniandy, Removal of organic pollutants from water by Fe2O3/TiO2 based photocatalytic degradation: a review, Environ. Technol. Innov. 21 (2021), 101230, https://doi.org/10.1016/j.eti.2020.101230.

[12] M. Zahid Hussain, Z. Yang, A.M.E. Khalil, S. Hussain, S.U. Awan, Q. Jia, R. A. Fischer, Y. Zhu, Y. Xia, Metal-organic framework derived multi-functionalized and co-doped TiO2/C nanocomposites for excellent visible-light photocatalysis, J. Mater. Sci. Technol. 101 (2022) 49–59, https://doi.org/10.1016/j.jmst.2021.05.052.

[13] R. Yadav, T.S. Chundawat, P.K. Surolia, D. Vaya, Photocatalytic degradation of textile dyes using β-CD-CuO/ZnO nanocomposite, J. Phys. Chem. Solids 165 (2022), 110691, https://doi.org/10.1016/j.jpcs.2022.110691.

[14] M. Malika, S.S. Sonawane, Statistical modelling for the ultrasonic photodegradation of rhodamine B dye using aqueous based Bi-metal doped TiO2 supported montmorillonite hybrid nanofluid via RSM, Sustain. Energy Technol. Assessments. 44 (2021), 100980, https://doi.org/10.1016/j.seta.2020.100980.

[15] Z. Sun, J. Fan, R. Feng, M. Wang, Y. Zhou, L. Zhang, Facile preparation of hierarchical heterostructured TiO2/bi/Bi2MoO6 photocatalyst for phocatalytic degradation of toluene gas, J. Chem. Technol. Biotechnol. 96 (2021) 1732–1741, https://doi.org/10.1002/jctb.6698.

[16] N. Riaz, M. Hassan, M. Siddique, Q. Mahmood, U. Farooq, R. Sarwar, M.S. Khan, Photocatalytic degradation and kinetic modeling of azo dye using bimetallic photocatalysts: effect of synthesis and operational parameters, Environ. Sci. Pollut. Res. 27 (2020) 2992–3006, https://doi.org/10.1007/s11356-019-06727-1.

[17] P.A.K. Reddy, B. Srinivas, P. Kala, V.D. Kumari, M. Subrahmanyam, Preparation and characterization of Bi-doped TiO2 and its solar photocatalytic activity for the degradation of isoproturon herbicide, Mater. Res. Bull. 46 (2011) 1766–1771, https://doi.org/10.1016/j.materresbull.2011.08.006.

[18] T.S. Natarajan, K. Natarajan, H.C. Bajaj, R.J. Tayade, Enhanced photocatalytic activity of bismuth-doped TiO2 nanotubes under direct sunlight irradiation for degradation of rhodamine B dye, J. Nanopart. Res. 15 (2013) 1669, https://doi.org/10.1007/s11051-013-1669-3.

[19] J.-H. Shen, H.-Y. Chuang, Z.-W. Jiang, X.-Z. Liu, J.-J. Horng, Novel quantification of formation trend and reaction efficiency of hydroxyl radicals for investigating photocatalytic mechanism of Fe-doped TiO2 during UV and visible light-induced degradation of acid orange 7, Chemosphere. 251 (2020), 126380, https://doi.org/10.1016/j.chemosphere.2020.126380.

[20] P.K. Surolia, R.J. Tayade, R.V. Jasra, Effect of anions on the photocatalytic activity of Fe(III) salts impregnated TiO2, Ind. Eng. Chem. Res. 46 (2007) 6196–6203, https://doi.org/10.1021/ie0702678.

[21] G. Zhao, J. Zou, C. Li, J. Yu, X. Jiang, Y. Zheng, W. Hu, F. Jiao, Enhanced photocatalytic degradation of rhodamine B, methylene blue and 4-nitrophenol under visible light irradiation using TiO2/MgZnAl layered double hydroxide, J. Mater. Sci. Mater. Electron. 29 (2018) 7002–7014, https://doi.org/10.1007/s10854-018-8687-y.

[22] N. Chakinala, P.R. Gogate, C.A. Gupta, Highly efficient bi-metallic bismuth-silver doped TiO2 photocatalyst for dye degradation, Korean J. Chem. Eng. 38 (2021) 2468–2478, https://doi.org/10.1007/s11814-021-0890-5.

[23] R.J. Tayade, P.K. Surolia, R.G. Kulkarni, R.V. Jasra, Photocatalytic degradation of dyes and organic contaminants in water using nanocrystalline anatase and rutile TiO2, Sci. Technol. Adv. Mater. 8 (2007) 455–462, https://doi.org/10.1016/j.stam.2007.05.006.

[24] R.J. Tayade, P.K. Surolia, M.A. Lazar, R.V. Jasra, Enhanced photocatalytic activity by silver metal ion exchanged NaY zeolite Photocatalysts for the degradation of organic contaminants and dyes in aqueous medium, Ind. Eng. Chem. Res. 47 (2008) 7545–7551, https://doi.org/10.1021/ie800441c.

[25] S. Bagwasi, B. Tian, J. Zhang, M. Nasir, Synthesis, characterization and application of bismuth and boron co-doped TiO2: a visible light active photocatalyst, Chem. Eng. J. 217 (2013) 108–118, https://doi.org/10.1016/j.cej.2012.11.080.

[26] F.M. Bautista, J.M. Campelo, A. Garcia, D. Luna, J.M. Marinas, M.C. Moreno, A. A. Romero, J.A. Navio, M. Macias, Structural and textural characterization of AlPO4-B2O3 and Al2O3-B2O3 (5-30 wt% B2O3) systems obtained by boric acid impregnation, J. Catal. 173 (1998) 333–344, https://doi.org/10.1006/jcat.1997.1905.

[27] S. Landi, I.R. Segundo, E. Freitas, M. Vasilevskiy, J. Carneiro, C.J. Tavares, Use and misuse of the Kubelka-Munk function to obtain the band gap energy from diffuse reflectance measurements, Solid State Commun. 341 (2022) 1–7, https://doi.org/10.1016/j.ssc.2021.114573.

[28] S. Rengaraj, X.Z. Li, P.A. Tanner, Z.F. Pan, G.K.H. Pang, Photocatalytic degradation of methylparathion - an endocrine disruptor by Bi3+−doped TiO2, J. Mol. Catal. A Chem. 247 (2006) 36–43, https://doi.org/10.1016/j.molcata.2005.11.030.

[29] M. Moradi, F. Khorasheh, A. Larimi, Pt nanoparticles decorated bi-doped TiO2 as an efficient photocatalyst for CO2 photo-reduction into CH4, Sol. Energy 211 (2020) 100–110, https://doi.org/10.1016/j.solener.2020.09.054.

[30] G. Botelho, J. Andres, L. Gracia, L.S. Matos, E. Longo, Photoluminescence and photocatalytic properties of Ag3PO4 microcrystals: an experimental and theoretical investigation, Chempluschem. 81 (2016) 202–212, https://doi.org/10.1002/cplu.201500485.

[31] S.P. Ghorpade, N. Kottamb, R. Melavankice, N.R. Patil, Photoluminescence, TGA/DSC and photocatalytic activity studies of Dy3+ doped SrY2O4 nanophosphors, RSC Adv. 10 (2020) 21049–21056, https://doi.org/10.1039/D0RA03094E.

[32] B.P. Maheshwary, R.A. Singh, Singh, color tuning in thermally stable Sm3+− activated CaWO4 nanophosphors, New J. Chem. 39 (2015) 4494–4507, https://doi.org/10.1039/C4NJ01911C.

[33] Ş.Ş. Türkyılmaz, N. Güy, M. Özacar, Photocatalytic efficiencies of Ni, Mn, Fe and ag doped ZnO nanostructures synthesized by hydrothermal method: the synergistic/antagonistic effect between ZnO and metals, J. Photochem. Photobiol. A Chem. 341 (2017) 39–50, https://doi.org/10.1016/j.jphotochem.2017.03.027.

[34] H. Moradi, A. Eshaghi, S.R. Hosseini, K. Ghani, Fabrication of Fe-doped TiO2 nanoparticles and investigation of photocatalytic decolorization of reactive red 198 under visible light irradiation, Ultrason. Sonochem. 32 (2016) 314–319, https://doi.org/10.1016/j.ultsonch.2016.03.025.

[35] P.K. Surolia, R.V. Jasra, Photocatalytic degradation of p-nitrotoluene (PNT) using TiO2-modified silver-exchanged NaY zeolite: kinetic study and identification of mineralization pathway, Desalin. Water Treat. 57 (2016) 22081–22098, https://doi.org/10.1080/19443994.2015.1125798.